RSC Advances

PAPER

View Article Online
View Journal | View Issue

Cite this: *RSC Adv.*, 2017, **7**, 12959

System-wide analysis of manganese starvation-induced metabolism in key elements of *Lactobacillus plantarum*

Yanjun Tong,[a] Qixiao Zhai,[ad] Gang Wang,[ad] Qiuxiang Zhang,[a] Xiaoming Liu,[ad] Fengwei Tian,[ad] Jianxin Zhao,[acd] Hao Zhang[acd] and Wei Chen*[abcd]

To analyze the response mechanisms of *Lactobacillus plantarum* against manganese starvation stress, different metabolisms from physiology, proteomics and transporters aspects in *L. plantarum* CCFM 436 were systematically investigated. The kinetics of cell growth (μ_{max}) decreased from 0.310 to 0.256 h^{-1}, while thinner cell morphology was observed by transmission electron microscopy under Mn-starvation conditions. Gas chromatography-mass spectrometry analysis indicated that membrane mobility and compactness increased, with a higher proportion of unsaturated fatty acids and cyclopropane fatty acids. High-performance liquid chromatography analysis showed that intracellular Asp, Glu, and Arg contents, closely related to energy metabolism, were significantly increased. Fourier transform infrared spectroscopy proved that some functional groups (N–H and O=C–OH) were significantly affected by Mn starvation. Comparative two-dimensional proteomic analysis identified 73 proteins that differed significantly under Mn starvation conditions. These differentially expressed proteins involved in carbohydrate, amino acid and transcription/translation metabolisms and stress response were categorized as crucial components required to resist manganese starvation stress. Moreover, qRT-PCR analysis proved that MntH 1–5, negatively regulated by MntR, acted as potential Mn importers under Mn starvation conditions. The proposed coordinated mechanism model provides a reference for, and insight into, the intracellular metabolism of LAB strains.

Received 3rd January 2017
Accepted 10th February 2017

DOI: 10.1039/c7ra00072c

rsc.li/rsc-advances

1. Introduction

Manganese is an essential element of life and acts as "cell security" or a "life bodyguard".[1–3] Manganese is a component in a variety of enzymes with important physiological functions, such as manganese-superoxide dismutase, arginase and pyruvate carboxylase.[4,5] Manganese also acts as a cofactor in some metalloenzymes, such as aminopeptidase, dipeptidase, manganese catalase, D-xylose isomerase, L-arabinose isomerase and ribozymes.[3,4] Manganese must be maintained at an appropriate level in organisms; otherwise, stress can result from manganese starvation or excess.[1] It is important to maintain a steady-state balance in the regulation of manganese to ensure normal physiological function.

Lactobacillus plantarum (*L. plantarum*) is a probiotic that can effectively reduce heavy metal ion toxicity.[6–10] In particular, *L. plantarum* requires a relatively high level of manganese ions for optimal growth due to the absence of superoxide dismutase.[11,12] Manganese is an essential element in the growth of lactic acid bacteria, not only involved in the composition of some enzymes, such as lactate dehydrogenase, but also promoting the production of certain enzymes to assist cellular metabolism.[11] Manganese ions are indispensable to the stability and function of the metal protein, affecting the biological function of these proteins. These metalloproteins and metalloenzymes are involved in the regulation of homeostasis, electron transport, biomolecule synthesis, biological substance transport, oxidative stress, signal transduction, gene regulation and other functions.[11,13,14] Therefore, the steady-state regulation of manganese is important in maintaining the normal physiological function of intracellular manganese ions. However, decreasing heavy metal ion toxicity has been the focus of most research in this area.[15–18] Although manganese ion studies have focused on individual features, resistance to manganese starvation stress has not been studied systematically. Understanding the molecular mechanisms of the response to manganese starvation will be helpful in elucidating the

[a]*State Key Laboratory of Food Science and Technology, School of Food Science and Technology, Jiangnan University, Wuxi 214122, People's Republic of China. E-mail: tongyanjun@jiangnan.edu.cn; chenwei66@jiangnan.edu.cn*

[b]*Beijing Innovation Centre of Food Nutrition and Human Health, Beijing Technology & Business University, Beijing 100048, People's Republic of China*

[c]*International Joint Research Center for Probiotics & Gut Health, Jiangnan University, Wuxi 214122, P.R. China*

[d]*International Joint Research Laboratory for Probiotics at Jiangnan University, People's Republic of China*

physiological mechanisms of this kind of probiotic against manganese starvation stress from a different angle.

Our previous has shown the strong potential of *L. plantarum* CCFM436 to reduce manganese toxicity.[19] Herein, *L. plantarum* CCFM436 was used to study metabolic response mechanisms under manganese starvation stress by investigating cell physiology, proteomics and levels of key transport proteins.

2. Materials and methods

2.1 Microbial growth conditions

L. plantarum CCFM436, which was screened from wine cake samples of Shanlan wine from Hainan, China, was cultured in modified MRS broth at 37 °C for 18 h (Table 1). The manganese ion concentration in the MRS broth was 16 mg L^{-1}, while MRS broth without added $MnSO_4 \cdot H_2O$ was used to induce manganese starvation stress. The biomass at different culture phases was determined as the optical density at 600 nm (OD_{600}).

2.2 Analysis of cell physiology under manganese starvation conditions

2.2.1 Analysis of cell morphology using transmission electron microscopy (TEM). A 5 mL cultured medium was sampled and treated with glutaraldehyde at 4 °C for 0.5 h. The cells were centrifuged at 6000 × *g* for 5 min and then immobilized with agar. The agar-cell slice samples were soaked in phosphate buffer containing 2.5% glutaraldehyde and then transferred into osmium tetroxide solution. The slices were treated with uranyl acetate solution after being washed with double-distilled H_2O (ddH_2O). The slices were dehydrated with ethanol and propylene oxide, respectively, and then stained with uranyl acetate. After implanting the slices into epoxy, the cell morphology of the sample was observed with a transmission electron microscope (Hitachi-H 7000, Tokyo, Japan).

2.2.2 Analysis of membrane fatty acids composition by gas chromatography-mass spectrometry (GC-MS). Cells (1.0 g) were collected by centrifugation at 6000 × *g* for 5 min and dissolved in 1.0 M NaOH–methanol (2.5 mL) and incubated at 70 °C for 2 h. After cooling to room temperature, a solution of 25% BF_3–methanol (2.5 mL) was added to the sample after cooling to room temperature, and the mixed sample was incubated at 65 °C for 2 h. The sample was again cooled at 20 °C for 10 min, and then 2 mL each of *n*-hexane and saturated NaCl solution was added sequentially and vortexed for 1 min. After centrifugation at 380 × *g* for 1 min, redundant water was removed with a moderate amount of anhydrous Na_2SO_4, and the supernatant oil was collected. The fatty acid composition was assayed using a trace GC-MS instrument (1200 L, Varian, Palo Alto, CA).

2.3 Analysis of intracellular amino acid composition and functional groups under manganese starvation conditions

2.3.1 Analysis of amino acid composition by high performance liquid chromatography (HPLC). A 50 mL sample of cultured medium was centrifuged at 8000 × *g* for 10 min. The collected thallus was washed three times with ddH_2O and its weight recorded. The collected thallus was then treated with 5% trichloroacetic acid in a 25 mL volumetric flask at 25 °C for 1 h. The lysis solutions were filtrated and the mother liquor centrifuged at 12 000 × *g* for 10 min, after which the supernatants were used to analyze the intracellular amino acid by HPLC.

2.3.2 Analysis of functional groups by Fourier transform infrared spectroscopy (FTIR). Different dried cell samples (approx. 2 mg) and KBr (200 mg) were repeatedly ground in an agate mortar. The sample was collected and turned into a thin cylinder using a press. The cylinder was measured in the wavelength region 400–4000 cm^{-1} using a Fourier transform infrared spectrometer (NEXUS, Nicolet, USA).

2.4 Two-dimensional (2D) gel electrophoresis

2.4.1 Isolation of whole proteins. Bacterial cells with different manganese concentrations were centrifuged at 6000 × *g* for 10 min and washed three times with phosphate buffer for proteomic study. Thalli were resuspended in enzymatic lysis buffer with mutanolysin (7 M urea, 2 M thiourea and 40% CHAPS, 40 mM Tris-base with 40 mM dithiothreitol, 1 mM phenylmethane sulfonyl fluoride, 2% immobilized pH gradient buffer (pH 3–10), protease inhibitor and nuclease mix) at 37 °C for 2 h and then sonicated for 15 min on ice. The lysate was then centrifuged at 12 000 × *g* for 30 min at 4 °C so that the supernatants contained the whole protein from the samples. The Bradford assay was used to determine protein concentrations.

2.4.2 2D gel electrophoresis and image analysis. Samples containing proteins (1000 μg) were diluted in IPG strip rehydration buffer (9 M urea, 4% CHAPS, 1% immobilized pH gradient buffer (pH 3–10), 1% dithiothreitol and 0.002% bromophenol blue) and then loaded on IPG strips at pH 3–10. Isoelectric focusing was carried out at 20 °C on an IPGhor Isoelectric Focusing System using the optimal program. After focusing, the IPG strips were equilibrated at room temperature for 15 min in equilibration buffer (50 mmol L^{-1} Tris–HCl pH 8.8, 6 mol L^{-1} urea, 30% glycerol, 2% sodium dodecyl sulfate and 0.002% bromophenol blue) with the addition of 1% dithiothreitol, and for a further 15 min in the same

Table 1 Main characteristics of the targeted strain used in the study

Species	Strain	Microbial type	Optimal *T*/pH	Description and source
Lactobacillus plantarum	CCFM436	Lactic acid bacteria; chemoheterotroph	*T* 37 °C; pH 6.2–6.4	Wine cake sample of shanlan wine from Hainan, China

equilibration buffer with the addition of 2.5% indole-3-acetic acid. The equilibrated strips were transferred into homogeneous 12.5% sodium dodecyl sulfate-polyacrylamide gels for 2D electrophoresis. After separation, the 2D electrophoresis gels were stained using Coomassie Blue G250.

The stained gels (three independent analytical replicates for each manganese concentration) were scanned at 300 dpi with an image scanner and analyzed with PDQuest software. Briefly, spot detection was carried out using optimized setting values for spot intensity, spot area and saliency, as determined by applying real-time filters to minimize artifact detection. After spot detection, manual spot editing was carried out to remove artifacts that escaped the filtering process. Spots that showed significant intensity differences (>1.5-fold or <0.67-fold change) between samples with a P value of <0.05 in different manganese concentrations were considered differentially expressed proteins.

2.4.3 MS analysis. Different protein spots were manually excised from the gels, washed with ddH_2O and destained in buffer (100 mM NH_4HCO_3 in 30% acetonitrile) three times. Protein spots were then vacuum dried. All protein spots were digested with 50 ng trypsin in 30 μL buffer (25 mM NH_4HCO_3 with the addition of 10% acetonitrile) at 37 °C for 20 h. The supernatants were transferred into a new tube and then vacuum dried. The dried peptides were dissolved in TCA buffer (0.1% TCA, 0.7 mg mL^{-1} α-cyano-4-hydroxy-*trans*-cinnamic acid in acetonitrile/TCA; 85 : 0.1 v/v). All respective peptides were spotted on the sample target plate and analyzed by MALDI-TOF/TOF mass spectrometry. Peptides digested with trypsin were analyzed in positive ion mode, and the spectra were adjusted by peptide calibration. The spectra were analyzed using FlexAnalysis and BioTools software. The peptide results were compared and analyzed with the following parameters: NCBI-nr bacteria database, trypsin as the digestion enzyme, acceptance of cysteine carbamidomethylation, methionine oxidation, fragment mass tolerance of 0.99 Da and peptide mass tolerance of 300 ppm.

2.5 Quantitative RT-PCR

Quantitative RT-PCR analysis was used to quantify protein transcription. Total RNA was extracted from different samples with Trizol reagent according to manufacturer instructions. The RNA concentration was determined, and reverse transcription reactions were carried out with a PrimeScript RT Reagent Kit with gDNA Eraser. Then, 10 μL of a genome DNA removal mixture, containing 1 μg extracted total RNA, 2 μL 5 × DNA eraser buffer, 1 μL gDNA eraser and RNase-free dH_2O, was added. The reaction was carried out at 42 °C for 2 min, and the RT-PCR reaction was processed using a 20 μL mixture (1 μL PrimeScript RT enzyme mix, 1 μL RT primer mix, 4 μL 5 × PrimeScript buffer, 4 μL RNase free dH_2O, and 10 μL of the reaction mixture for genome DNA removal). qRT-PCR was performed using SYBR Premix Ex Taq II. The 20 μL PCR reaction mixture contained 10 μL SYBR Premix Ex Taq II, 1 μL PCR forward primer (10 μM), 1 μL PCR reverse primer (10 mM), 1 μL sample cDNA and 7 μL dH_2O. PCR specificity was verified by melt-curve analysis of the samples. The cycle threshold (C_t) value was measured, and the relative quantification of specific gene expressions was determined using the $2^{-\Delta\Delta C_t}$ method. Primers are listed in Table 2. 16S rRNA of *L. plantarum* CCFM436 was used as an internal control for PCR amplification.

Table 2 Primer sequences used for qRT-PCR experiments

Primer	Sequence (5′-3′)	Production (bp)
MntH-1-F	TCACCGTGGCATACAGTGACACAC	187
MntH-1-R	TGAAATTGTTTTAGCGCACGACCT	
MntH-2-F	TACGTGGCATGTCGATGATGG	203
MntH-2-R	CACGACCGTCGTCGTCATCATATC	
MntH-3-F	TACATGGATCCCGGTAACTGGTCAAC	145
MntH-3-R	GATCCATCTGACTCACGATACCAAG	
MntH-4-F	GATAGTAAGAGCTTGGACGAAGTC	225
MntH-4-R	CCATGGCTTGTAGCAACATGGCAAT	
MntH-5-F	GCAGTCGGCTATATGGATCCCGGCAAC	246
MntH-5-R	CATATCAGTCGCCATCATCGCGAC	
MntR-F	TATTTTCGAGCTTGGTGGTACGAA	218
MntR-R	CTAAGAAATCTTCCCAGATTCGGTG	
16S rRNA-F	AGCAGCCGCGGTAATACGTAGGTG	227
16S rRNA-R	GACCAGACAGCCGCCTTCGCCACAC	

3. Results and discussion

3.1 Effects of manganese starvation on growth performance

Manganese is an essential element for cell growth and is involved in a variety of metabolic pathways. The growth of *L. plantarum* CCFM436 was inhibited by manganese starvation stress, as indicated by the lower OD values. Cell performance is shown in Fig. 1A. The final OD_{600} was 5.27 in MRS culture and 2.37 under manganese starvation stress. Similarly, μ_{max} changes occurred with cell growth (see Fig. 1B). The μ_{max} of the cells decreased from 0.310 to 0.256 h^{-1} under manganese starvation conditions. Moreover, the μ_{max} peak time was significantly delayed, and the appearance time for μ_{max} extended from 5.0 to 8.5 h. Growth was clearly limited, as observed in a previous report, in which the growth of *L. plantarum* NC8 was directly correlated with the amount of manganese ions in the medium.[11] The highest OD_{600} was reached at microtiter scale at the highest manganese ion concentration tested. As manganese can participate as an enzyme cofactor in various biological processes, manganese starvation was harmful to the growth of *L. plantarum* CCFM436. However, slight cell growth was observed in complex media (*e.g.*, MRS) without manganese addition. This may be caused by the yeast extract, beef extract or trypsin powder used containing trace amounts of manganese that could be used for cell growth.[11]

3.2 Effects of manganese starvation stress on cell physiology

3.2.1 Cell morphology under manganese starvation stress. As the primary barrier, cell morphology is crucial in maintaining cell viability and metabolic function, particularly under environmental stress.[18,20] Cell integrity is necessary to maintain

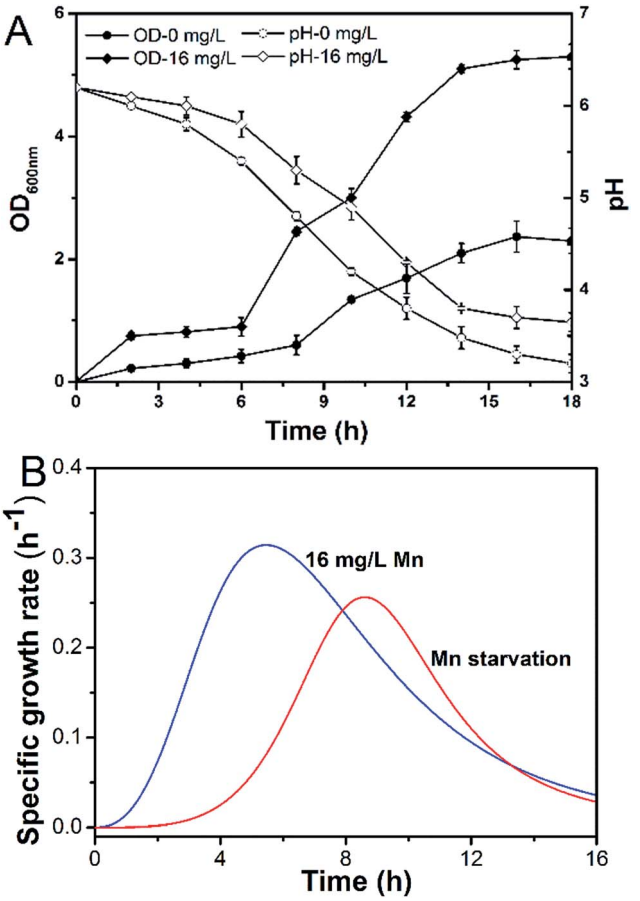

Fig. 1 Effect of Mn starvation on growth kinetics of *L. plantarum* CCFM 436: (A) pH/biomass (OD_{600}) and (B) μ.

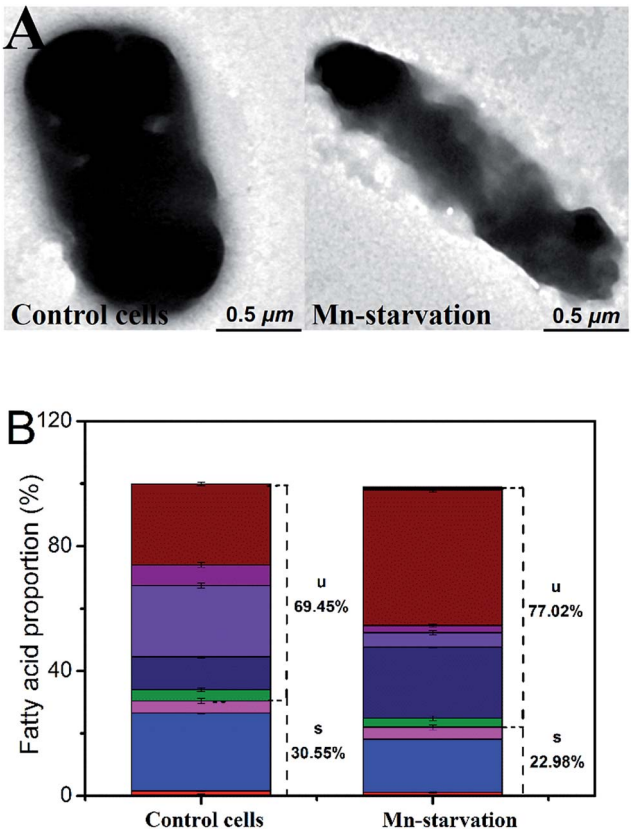

Fig. 2 Effect of Mn starvation on cell physiology of *L. plantarum* CCFM 436: (A) cell morphology and (B) cell membrane fatty acid composition. Fatty acids in colored bars, from bottom to top, are C12:0, C14:0, C16:0, C18:0, C16:1, C18:1, C18:1 (*trans*-1,3-octadecenoic acid), C18:2, C19-cyc and unidentified fatty acids, respectively.

the normal physiological function of cells and is essential for keeping intracellular biochemical reactions steady. As shown in Fig. 2A, compared with that of *L. plantarum* CCFM436 grown in normal MRS, the cell morphology of *L. plantarum* CCFM436 grown under manganese starvation had lower integrity. The cell membrane was also thinner. This cell shrinkage behavior might be beneficial for saving energy to better resist environmental stress.

3.2.2 Fatty acid composition of cell membrane under manganese starvation stress. As another main mechanical barrier, the cell membrane can defend against external stress by adjusting its fatty acid composition.[21] The saturated fatty acids in *L. plantarum* CCFM436 were lauric (C12:0), myristic (C14:0), palmitic (C16:0) and stearic acids (C18:0), whereas the unsaturated acids were hexadecenoic (C16:1), oleic (C18:1), *trans*-13-octadecenoic (C18:1), linoleic (C18:2) and cyclopropane fatty acids (C19-cyc) (Fig. 2B). Unsaturated fatty acids dominated the fatty acid composition at all manganese levels. The proportion of unsaturated fatty acids increased from 69.45% to 77.02% under the manganese starvation conditions, which suggested that the higher proportion of unsaturated fatty acids in the cell membrane might contribute to adaption to the external environment. Furthermore, the ratio of saturated fatty acids to unsaturated fatty acids could indirectly reflect the mobility of the cell membrane. The unsaturated fatty acid content in the cell membrane of *L. plantarum* CCFM436 increased under manganese starvation conditions, causing cell membrane fluidity to increase. A higher proportion of unsaturated fatty acids is closely associated with certain types of metabolism (nutrient transport and exchange).[22]

Meanwhile, the cyclopropane fatty acid content was much higher under manganese starvation stress conditions (increased from 25.82% to 43.54%), whereas that of octadecenoic acid was significantly lower. High cyclopropane fatty acid contents have been reported as beneficial to maintaining better membrane compactness and resistance to harmful environmental factors.[20,21]

3.3 Intracellular amino acid composition and key functional groups under manganese starvation stress

3.3.1 Intracellular amino acid composition under manganese starvation stress. It has been suggested that amino acid metabolism plays an important role in regulating intracellular homeostasis, producing metabolic energy and enhancing the resistance of cells to environmental stress.[23] Due to the lack of a TCA cycle, the main ATP production method in *L. plantarum* is amino acid metabolism. Contents of Asp, Glu, Arg, Lys, Thr and

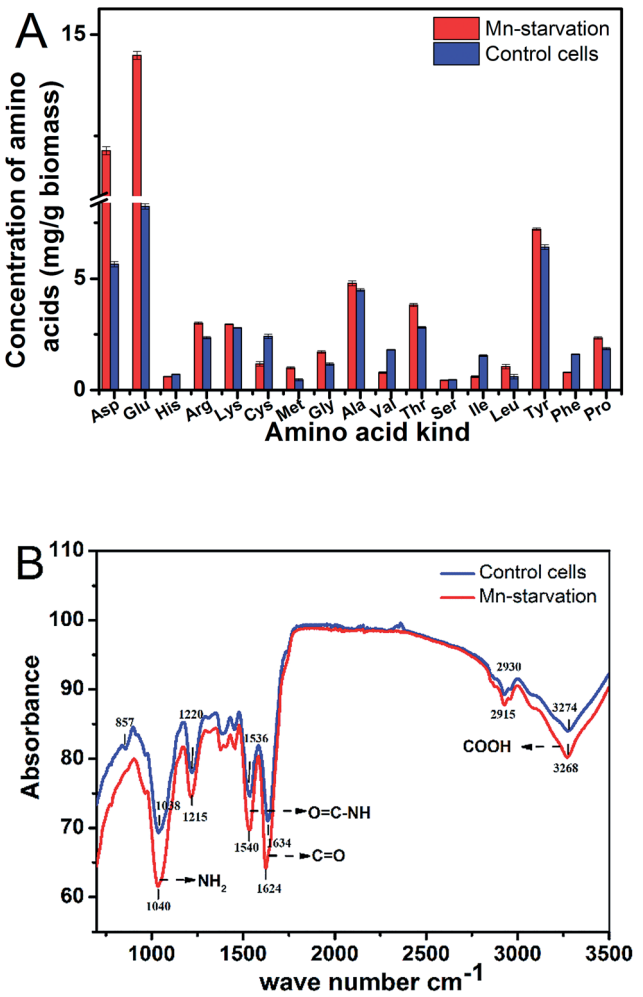

Fig. 3 Effect of Mn starvation on intracellular amino acid and functional groups of *L. plantarum* CCFM 436: (A) intracellular amino acids and (B) FTIR spectra analysis.

other amino acids were accumulated under manganese starvation stress (see Fig. 3A). Arg can be metabolized to produce ATP through the ADI pathway, while the decarboxylation reaction of Asp also provides energy for cellular growth.[24] Glu, Asp and Thr could also be translated to other amino acids, such as ornithine, alanine and proline, through a series of transamination and other reactions.[24] Arg and Lys have double amino groups, while Asp and Glu have double carboxyl groups. The increased contents of these amino acids demonstrated their close association with manganese adsorption of *L. plantarum* CCFM436 from another point of view, which was consistent with our previous reports. Meanwhile, the Cys and Ile contents decreased. Cys can be degraded into pyruvic acid and hydrogen sulfide under aerobic conditions. Ile, belonging to the branched chain amino acid (BCAA), can be swiftly consumed and provide energy to maintain cell metabolism under environmental stress.[24]

3.3.2 Key functional groups under manganese starvation condition. FTIR spectroscopy was employed to analyze changes in functional groups on the cell surface under manganese starvation conditions (see Fig. 3B). The FTIR spectrum of cells from normal MRS medium displayed absorption peaks at 1038, 1220, 1536, 1634, 2915 and 3274 cm^{-1}. Comparatively, those under manganese starvation stress afforded more complex peaks due to the increased number of derivatives in normal MRS. In the Mn-starvation medium, the main characteristic absorption peaks of strain CCFM436 were stable, with several peaks associated with specific functional groups (1038, 1536, 1634 and 3274 cm^{-1}) having moved slightly. The most fluctuation was associated with carboxyl and amino groups, which was caused by manganese deficiency. Fluctuation of the absorption peaks at 1634 cm^{-1} (C=O) and 3274 cm^{-1} (O=C–OH) was due to the change in stretching vibration of the carboxyl group without manganese ion complexation or the ion exchange effect.[25,26] Similarly, movement of the peaks at 1038 and 1536 cm^{-1} indicated N–H fluctuation and the generation of some different compounds when the functional amino group of the protein did not uptake manganese ions.[26,27] These results were also consistent with the main chemical bond activations in the Mn bioadsorption process (such as C=O stretching, N–H bending, and O–H stretching).[27]

3.4 Proteomic analysis and functional classification of identified proteins

3.4.1 Carbohydrate and nitrogen metabolism. To understand the protein expression of *L. plantarum* CCFM436 under manganese starvation stress, 2D electrophoresis was used to analyze the proteomics of whole cell proteins. The protein spots of *L. plantarum* CCFM436 were mainly located in the acidic and neutral regions. Protein profiles were analyzed by Quest software. The different protein spots were identified by MALDI-TOF/TOF/MS, and results are shown in Fig. 4 and Table 3. Among the 73 different protein spots, 19, 2, and 7 protein spots were involved in carbohydrate metabolism, amino acid and nitrogen metabolism, and nucleotide metabolism, respectively. Twenty-three protein spots participated in the transcription and

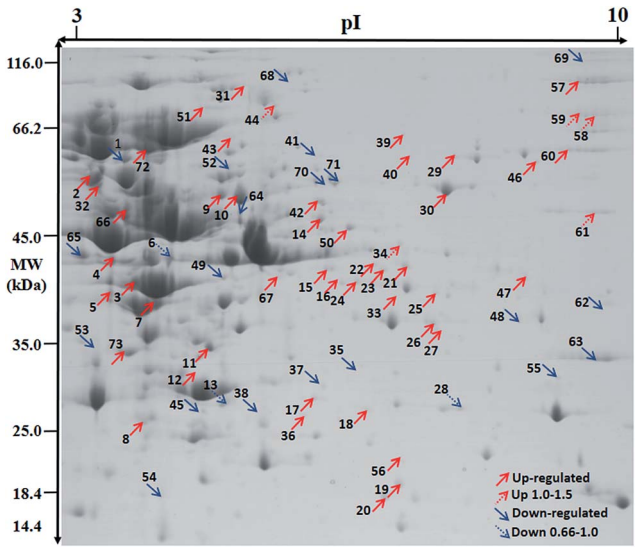

Fig. 4 Effect of Mn starvation on overall protein expression of *L. plantarum* CCFM 436 *via* proteome analysis.

Table 3 Identification of differentially expressed proteins with different levels of manganese in *L. planturam* CCFM436 by MALDI-TOF/TOF analysis

Spot	Accession	Protein name	Theoretical MW (Da)	MASCOT score	No. matched	Fold change 0/16
Carbon metabolism						
2	gi|489735124	F_0F_1 ATP synthase subunit beta	50 786	395	7(1)	1.63
3	gi|334880343	D-Lactate dehydrogenase (D-LDH)	37 176	321	8(2)	3.86
6	gi|5823364	PepQ	41 316	387	5(3)	0.84
7	gi|3043367	L-Lactate dehydrogenase	34 256	90	2(0)	2.48
8	gi|334881845	Ribose-5-phosphate isomerase A	24 617	217	4(1)	2.66
9	gi|334880734	NADH peroxidase	48 443	560	9(6)	2.44
10	gi|489733775	Glyceraldehyde-3-phosphate dehydrogenase	36 645	148	2(1)	1.83
12	gi|489733459	Fructose-bisphosphate aldolase	31 060	851	9(7)	1.76
16	gi|334881745	Phosphoglycerate dehydrogenase	34 635	82	1(1)	4.27
30	gi|334881069	Acetaldehyde dehydrogenase	49 062	280	5(2)	3.20
34	gi|13940254	Acetate kinase	43 870	364	6(4)	1.20
45	gi|489735713	Phosphoglyceromutase	26 069	504	7(3)	0.34
47	gi|334882090	ATP synthase gamma chain	34 586	225	3(2)	5.33
53	gi|300494598	Triose-phosphate isomerase	25 858	268	3(2)	0.13
59	gi|489734188	Phosphoenolpyruvate-protein phosphotransferase	63 271	67	1(1)	1.28
65	gi|334880497	Putative manganese-dependent inorganic pyrophosphatase	33 645	563	7(3)	0.36
66	gi|489735164	Glucose-6-phosphate isomerase	49 776	156	2(1)	2.47
67	gi|334880778	Ferredoxin-NADP reductase (FNR) (Fd-NADP + reductase)	36 231	251	5(1)	2.05
68	gi|254046929	Putative phosphoketolase	90 611	96	2(1)	0.30
Nitrogen and amino acid metabolism						
28	gi|334881598	Putative protein-tyrosine phosphatase	29 819	522	7(4)	0.97
70	gi|334881735	Cysteine desulfurase	44 929	114	2(0)	0.34
Nucleotide metabolism						
26	gi|334882300	Ribose-phosphate pyrophosphokinase	35 709	368	6(2)	2.41
35	gi|334881576	Dihydroorotate dehydrogenase	31 458	154	3(1)	0.49
44	gi|489733564	CTP synthase	59 728	242	6(0)	1.08
48	gi|339638332	GMP reductase	35 531	98	2(0)	0.09
50	gi|334881578	Carbamoyl-phosphate synthase pyrimidine-specific small chain	40 289	366	8(1)	84.63
56	gi|544928213	Nucleoside-triphosphate diphosphatase	21 831	142	2(2)	3.27
64	gi|334881512	Adenylosuccinate synthetase	47 453	395	6(3)	0.53
Transcription						
4	gi|328813989	DNA-directed RNA polymerase alpha chain	29 284	195	2(2)	2.43
25	gi|334881701	Primosomal protein DnaI	35 367	158	2(1)	2.41
32	gi|489733165	DNA polymerase III subunit beta	41 439	345	6(2)	1.69
41	gi|334881375	Chromosomal replication initiator protein dnaA	51 385	185	2(1)	1.60
46	gi|334881483	Uncharacterized RNA methyltransferase lp_3226	53 759	316	4(2)	1.76
61	gi|489733582	DEAD/DEAH box helicase	58 875	146	3(1)	0.69
69	gi|640538996	DNA-directed RNA polymerase subunit beta'	135 760	283	5(2)	0.26
Translation						
1	gi|339638926	Ribosomal protein S1	47 212	404	5(3)	0.61
11	gi|334881031	L-2-Hydroxyisocaproate dehydrogenase	34 810	280	4(2)	2.91
15	gi|489734520	Methionyl-tRNA formyltransferase	34 473	37	6(3)	2.29
29	gi|334881840	Glutamyl-tRNA synthetase	57 050	442	7(5)	2.59
38	gi|334881788	Ribosomal protein S30EA	21 698	351	3(3)	0.38
42	gi|334882268	Elongation factor Tu (EF-Tu)	43 378	138	2(1)	3.20
43	gi|334882897	Arginyl-tRNA synthetase	63 003	71	1(1)	2.43
49	gi|489734874	30S ribosomal protein S2	30 208	250	4(1)	0.15
51	gi|334881700	Threonyl-tRNA synthetase	73 784	256	4(2)	4.76
52	gi|334882583	Aspartyl/glutamyl-tRNA (Asn/Gln) amidotransferase subunit B (Asp/Glu-ADT subunit B)	53 315	259	5(2)	0.37
58	gi|334880391	Aspartyl-tRNA synthetase	68 060	105	2(1)	1.24

Table 3 (*Contd.*)

Spot	Accession	Protein name	Theoretical MW (Da)	MASCOT score	No. matched	Fold change 0/16
54	gi|334881831	50S ribosomal protein L10	18 212	495	6(3)	0.29
55	gi|334881832	50S ribosomal protein L1	24 742	117	3(0)	0.18
57	gi|489733962	Elongation factor P	76 909	162	3(2)	2.02
62	gi|489734874	30S ribosomal protein S2	30 208	282	5(3)	0.25
63	gi|489733967	50S ribosomal protein L2	30 145	342	6(3)	0.13
Stress response						
19	gi|489735106	Universal stress protein UspA	17 728	445	4(4)	4.16
31	gi|334882861	ATP-dependent Clp protease, ATP-binding subunit ClpL	75 929	224	3(2)	1.89
71	gi|1552551	Catabolite control protein A	30 742	376	5(3)	0.64
72	gi|33312966	Heat shock protein	19 729	165	2(2)	27.26
73	gi|334881995	UPF0082 protein lp_2253	26 371	142	2(1)	1.75
Transporter						
14	gi|503121615	Glycine/betaine ABC transporter ATP-binding protein	44 005	225	3(2)	2.14
22	gi|334882144	Multiple sugar ABC transporter, ATP-binding protein	41 441	643	8(5)	3.13
24	gi|334882864	Oligopeptide ABC transporter, ATP-binding protein	36 667	353	7(4)	1.59
33	gi|489733642	PTS mannose transporter subunit IIAB	35 268	573	6(6)	2.19
36	gi|334883019	Glutamine ABC transporter, ATP-binding protein	26 811	189	2(2)	6.35
37	gi|334882691	Metal-dependent regulator	23 873	152	4(0)	0.50
60	gi|334882868	Oligopeptide ABC transporter, substrate binding protein	60 321	66	1(1)	6.01
Others						
5	gi|334880815	Lipoate-protein ligase	1201	262	4(2)	27.26
13	gi|334882009	2,3,4,5-Tetrahydropyridine-2,6-dicarboxylate *N*-acetyltransferase	24 552	282	3(2)	0.93
17	gi|334882348	Metallo-beta-lactamase	27 604	109	2(1)	2.07
18	gi|334881906	Putative uncharacterized protein	20 742	105	1(1)	6.94
20	gi|489733483	Hypothetical protein	18 207	246	3(1)	2.19
21	gi|300493552	Ribose-phosphate diphosphokinase	35 551			2.06
23	gi|334880640	Phosphate acyltransferase	37 400	293	4(2)	6.75
27	gi|334880612	3-Oxoacyl-[acyl-carrier-protein] synthase 3 protein 2	35 285	206	3(2)	2.23
40	gi|334882817	Poly(glycerol-phosphate) alpha-glucosyltransferase	57 597	198	4(2)	2.39
39	gi|334882270	Putative metallo-beta-lactamase superfamily protein	63 946	195	4(0)	1.77

translation process. Meanwhile, seven and five protein spots were associated with the transport system and stress response, respectively, and 10 protein spots were involved in other response processes.

Cellular metabolism and flow direction were essential to the growth of *L. plantarum* CCFM436. Nineteen proteins were involved in carbon metabolism under manganese starvation conditions, including glyceraldehyde-3-phosphate dehydrogenase (spot 10), fructose-2-phosphate aldolase (spot 12), phosphoglycerate (spot 16), glucose-6-phosphate isomerase (spot 66) and other proteins involved in the glycolysis pathway. As a type of facultative anaerobic bacteria, the glycolysis pathway is the main energy source of *L. plantarum* without a TCA cycle.[28,29] Meanwhile, tyrosine phosphatase and cysteine desulfurase participated in nitrogen metabolism, and CTP synthetase, dihydrolactate dehydrogenase and phosphate ribose pyrophosphate kinase were associated with nucleotide metabolism.

In terms of energy metabolism, the expression of some proteins involved in the glycolytic pathway for ATP synthesis were upregulated. For example, expression of glycosyl-bisphosphate aldolase (spot 12) and glyceraldehyde-3-phosphate dehydrogenase (spot 10) were upregulated 1.83-fold and 1.76-fold, respectively. The glycolytic pathway could be promoted through upregulation of these proteins. The expression of F_0F_1 ATP synthase beta (spot 2) and ATP synthase γ (spot 47) subunits, which are directly involved in the synthesis of ATP, were also upregulated 1.63-fold and 5.33-fold, respectively. Furthermore, the expression of ribose-5-phosphate isomerase (spot 8), which is involved in the pentose phosphate pathway, was also significantly increased, and its expression was upregulated 2.6-fold, indicating that pentose phosphate pathway activity was elevated under manganese starvation and provided more reduction power (NADPH) for the growth of *L. plantarum* CCFM436.

During amino acid metabolism, cysteine desulfurase (spot 70) catalyzed the desulfurization of cysteine to form alanine and enzyme-sulfide intermediates. The damage to superoxide ions in the cells could not be removed in time under manganese starvation conditions. Therefore, the expression of cysteine desulfurase was decreased, thereby increasing intracellular free cysteine content and regulating redox balance in the cells.[8]

3.4.2 Transcription and translation. Seventeen proteins participated in the transcription and translation process under manganese starvation conditions. The expression of chromosomal replication initiator protein DnaA (spot 41), DNA polymerase III subunit beta (spot 32) and DNA-directed RNA polymerase alpha chain (spot 4) were upregulated. Due to the functional association in tRNA synthesis, some proteins involved in aminoacyl-tRNA biosynthesis, such as glutamyl-tRNA synthetase (spot 29), arginyl-tRNA synthetase (spot 43) and aspartyl-tRNA synthetase (spot 58), were upregulated, indicating that *L. plantarum* improved many biological pathways by activating the translational level. However, the expression of aspartyl/glutamyl-tRNA (Asn/Gln) amidotransferase subunit B (spot 52) was downregulated. The AtMTP family of genes encodes proteins of the cation diffusion facilitator (CDF) family, which has several members with roles in manganese tolerance and is implicated in the transport of manganese as a tolerance mechanism.[30] Furthermore, the expression of ribosomal proteins (spots 1, 54, 55, 62 and 63) was downregulated, whereas expression of EF-Tu (spot 42) and EF-P (spot 57) was upregulated, suggesting a decrease in protein synthesis. These elongation factors are mostly responsible for escorting aminoacyl tRNAs to the ribosome as they proceed along mRNA.[1,8] Nevertheless, these factors seem to have a chaperone-like function in the protein-folding process. The interaction between the ribosome and elongation factors complexed to aminoacyl tRNA is essential for controlling translational accuracy.[8] EF-Tu has been reported as a factor in the adhesion of *L. plantarum* to manganese.[29] The expression of ribosomal proteins and elongation factors changed, along with the possible enhancement of translation accuracy and protein folding.

3.4.3 Molecular chaperone and stress response metabolism. Several stress response proteins were identified through MS analysis, such as heat shock protein (HSP) (spot 72), universal stress protein UspA (spot 19), ATP-dependent Clp protease (spot 31) and UPF0082 protein (spot 73). As the group of functional proteins responsible for protein folding, HSPs are closely related to environmental stresses, such as heat and heavy-metal stress.[8,30] HSP (spot 72) and universal stress protein UspA (spot 19) were upregulated 26.26-fold and 4.16-fold, respectively, under manganese starvation conditions. Meanwhile, the expression of ATP-dependent Clp protease, which was involved in molecular chaperoning and corrected protein folding, or cleaved/degraded misfolded proteins, was upregulated 2.89-fold. This molecular chaperone and stress response protein could be involved in the repair or degradation of misfolded proteins to improve protein folding accuracy.[1,8]

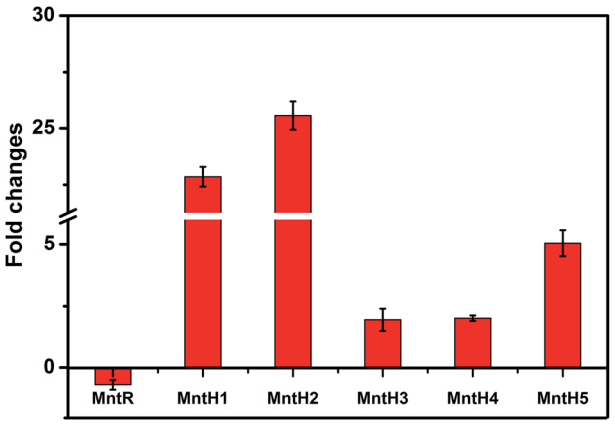

Fig. 5 Effect of Mn starvation on key related Mn transporters of *L. plantarum* CCFM 436.

3.5 Transcription analysis of manganese transporter genes using qRT-PCR

As the key regulator and defender in controlling intracellular steady-state manganese balance, the expression of manganese

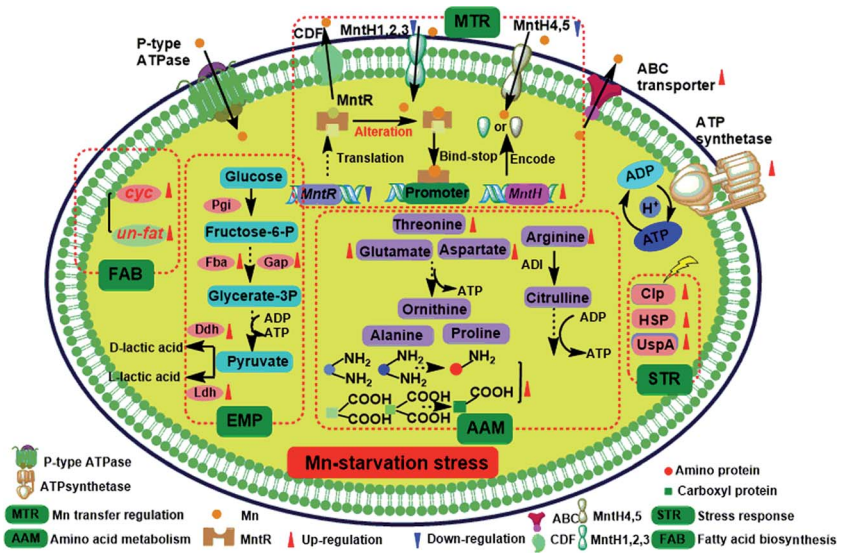

Fig. 6 Overview of the Mn starvation-induced metabolic changes in key elements of *L. plantarum* CCFM 436.

transporters is closely related to changes in manganese content.[31,32] However, identifying manganese transporters located in the membrane by 2D electrophoresis was difficult, so qRT-PCR analysis was performed instead (Fig. 5). Manganese uptake occurred through different types of cation transporters, with an active manganese ion transport system and five manganese transporters (MntH 1–5) identified in our previous study. The expression and regulation of manganese transporters were significantly different under manganese starvation stress. The transcription level of the manganese transporter regulator (MntR) was downregulated 0.69-fold, while those of manganese transporters (MntH 1–5) were upregulated. The transcription level of MntH 2 was upregulated more than 25-fold. The negatively regulation model between MntR and MntH was consistent with transcription levels changes in MntH 1–5 under 960 mg L^{-1} manganese stress (data not published). MntR is a transcriptional regulator that binds two Mn atoms in manganese-replete cells and then bonds with MntH promoters to form MntR:Mn_2. Therefore, the synthesis of manganese transporters can be downregulated. As the primary signal, Mn^{2+} can regulate the expression of Mn^{2+} transporters *via* Mn^{2+}-dependent repressor MntR.[31] The results suggest that MntH 1–5 were responsible for intracellular importation of manganese into *L. plantarum*, which acted as an importer under manganese starvation stress. It was necessary to acquire manganese to maintain normal *L. plantarum* metabolism. Mn starvation-induced metabolic changes to key elements in *L. plantarum* CCFM 436 are summarized in Fig. 6.

4. Conclusion

By analyzing cell physiology, proteomics and transporters, the response mechanisms of *L. plantarum* to Mn starvation stress were investigated. The results showed that μ_{max} decreased from 0.310 to 0.256 h^{-1}, TEM analysis indicated thinner cell morphology, and GC-MS analysis showed a higher proportion of unsaturated fatty acids and cyclopropane fatty acids, which improved the membrane fluidity and compactness. HPLC analysis of intracellular free amino acids indicated that intracellular Asp, Glu and Arg contents, which are closely related to energy metabolism, were increased. FTIR analysis showed that amino and carboxyl functional groups were significantly affected by the Mn starvation conditions. With comparative two-dimensional proteomic analysis, 73 proteins differentially expressed proteins involved in carbohydrate, amino acid and transcription/translation metabolisms, and stress response was identified under the Mn starvation conditions. Moreover, the potential Mn importer role of MntH 1–5 (negatively regulated by MntR) under Mn starvation stress was demonstrated using qRT-PCR analysis. The coordinated metabolism regulation model provides new insights into the response mechanism of probiotics under similar metal-starvation stress conditions.

Acknowledgements

This work was supported by State Key Program of National Natural Science Foundation of China (No. 31530056), the Science and Nature Foundation of Jiangsu Province (No. BK 20160169), the Jiangsu Province Postdoctoral Science Foundation Funded Project (No. 1601183C), the China Postdoctoral Science Foundation Funded Project (No. 2015M581727), the Program of Introducing Talents of Discipline to Universities (B07029), the Program for Changjiang Scholars and Innovative Research Team in University (IRT1249), and the Program of Collaborative innovation center of food safety and quality control in Jiangsu Province.

Notes and references

1 S. I. Hsieh, M. Castruita, D. Malasarn, E. Urzica, J. Erde, M. D. Page, H. Yamasaki, D. Casero, M. Pellegrini, S. S. Merchant and J. A. Loo, *Mol. Cell. Proteomics*, 2013, **12**, 65–86.
2 B. A. Eijkelkamp, C. A. McDevitt and T. Kitten, *BioMetals*, 2015, **28**, 491–508.
3 X. Zhang, H. H. Yang and Z. J. Cui, *RSC Adv.*, 2016, **6**, 27963–27968.
4 S. B. Schmidt, P. E. Jensen and S. Husted, *Trends Plant Sci.*, 2016, **21**, 622–632.
5 M. D. Angelis and M. Gobbetti, *Appl. Microbiol. Biotechnol.*, 1999, **51**, 358–363.
6 E. J. Gudiña, E. C. Fernandes, J. A. Teixeira and L. R. Rodrigues, *RSC Adv.*, 2015, **5**, 90960–90968.
7 J. N. Bhakta, K. Ohnishi, Y. Munekage, K. Iwasaki and M. Q. Wei, *J. Appl. Microbiol.*, 2012, **112**, 1193–1206.
8 H. An, F. P. Douillard, G. Wang, Z. Zhai, J. Yang, S. Song, J. Cui, F. Ren, Y. Luo, B. Zhang and Y. Hao, *Mol. Cell. Proteomics*, 2014, **13**, 2558–2572.
9 S. H. Ye, M. P. Zhang, H. Yang, H. Wang, S. Xiao, Y. Liu and J. H. Wang, *Carbohydr. Polym.*, 2014, **30**, 50–56.
10 S. Das, H. R. Dash and J. Chakraborty, *Appl. Microbiol. Biotechnol.*, 2016, **100**, 2967–2984.
11 N. Böhmer, S. König and L. Fischer, *FEMS Microbiol. Lett.*, 2013, **342**, 37–44.
12 L. C. Lew, M. T. Liong and C. Y. Gan, *J. Appl. Microbiol.*, 2012, **114**, 526–535.
13 L. Karaffa, R. Díaz, B. Papp, E. Fekete, E. Sándor and C. P. Kubicek, *Appl. Microbiol. Biotechnol.*, 2015, **99**, 7937–7944.
14 S. I. Hsieh, M. Castruita, D. Malasarn, E. Urzica, J. Erde, M. D. Page, H. Yamasaki, D. Casero, M. Pellegrini and S. S. Merchant, *Mol. Cell. Proteomics*, 2013, **12**, 65–86.
15 Q. X. Zhai, F. W. Tian, G. Wang, J. X. Zhao, X. M. Liu, K. Cross, H. Zhang, A. Narbad and W. Chen, *RSC Adv.*, 2016, **6**, 5990–9997.
16 J. L. Xing, G. Wang, Z. N. Gu, X. M. Liu, Q. X. Zhang, J. X. Zhao, H. Zhang, Y. Q. Chen and W. Chen, *RSC Adv.*, 2015, **5**, 37626–37634.
17 J. N. Bhakta, K. Ohnishi, Y. Munekage, K. Iwasaki and M. Q. Wei, *J. Appl. Microbiol.*, 2012, **112**, 1193–1206.
18 E. Dertli, M. J. Mayer and A. Narbad, *BMC Microbiol.*, 2015, **15**, 8–16.
19 Y. J. Tong, G. Wang, Q. X. Zhang, F. W. Tian, X. M. Liu, J. X. Zhao, H. Zhang and W. Chen, *RSC Adv.*, 2016, **6**, 102804–102813.

20 E. I. Urzica, A. Vieler, A. Hong-Hermesdorf, M. D. Page, D. Casero, S. D. Gallaher, J. Kropat, M. Pellegrini, C. Benning and S. S. Merchant, *J. Biol. Chem.*, 2013, **288**, 30246–30258.
21 Y. M. Zhang and C. O. Rock, *Nat. Rev. Microbiol.*, 2008, **6**, 222–233.
22 H. J. Hwang, S. P. Choi, S. Y. Lee, J. I. Choi, S. J. Han and P. C. Lee, *J. Biotechnol.*, 2015, **193**, 130–133.
23 K. Senouci-Rezkallah, P. Schmitt and M. P. Jobin, *Food Microbiol.*, 2011, **28**, 364–372.
24 P. Newsholme, L. Stenson, M. Sulvucci, R. Sumayao and M. Krause, *Compr. Biotechnol.*, 2011, **27**, 3–14.
25 K. M. H. Mata, O. M. Amaya, M. T. C. Barragan, F. J. A. Tapia and E. A. Felix, *Int. J. Photoenergy*, 2013, 578729.
26 A. Hernandez, D. Guzman and H. Garcia, *J. Appl. Microbiol.*, 2009, **107**, 395–403.
27 M. Feng, X. Chen, C. Li, R. Nurgul and M. Dong, *J. Food Sci.*, 2012, **77**, T111–T117.
28 M. F. Mazzeo, R. Lippolis, A. Sorrentino, S. Liberti, F. Fragnito and R. A. Siciliano, *PLoS One*, 2015, **10**, e0142376–0142389.
29 E. Vera Pingitore, A. Pessione, C. Fontana, R. Mazzoli and E. Pessione, *Int. J. Food Microbiol.*, 2016, **238**, 96–102.
30 E. Delhaize, B. D. Gruber, J. K. Pittman, R. G. White, H. Leung, Y. Miao, L. Jiang, P. R. Ryan and A. E. Richardson, *Plant J.*, 2007, **51**, 198–210.
31 T. E. Gunter, B. Gerstner, K. K. Gunter, J. Malecki, R. Gelein, W. M. Valentine, M. Aschner and D. I. Yule, *Neurotoxicology*, 2013, **34**, 118–127.
32 Z. Ma, F. E. Jacobsen and D. P. Giedroc, *Chem. Rev.*, 2009, **109**, 4644–4681.